LHCb-CONF-2024-003
June 5, 2024

Search for $B^{*0}_{(s)} \to \mu^+\mu^-$ in $B_c^+ \to \pi^+\mu^+\mu^-$ decays

LHCb collaboration[†]

Abstract

A search for the very rare $B^{*0} \to \mu^+\mu^-$ and $B_s^{*0} \to \mu^+\mu^-$ decays is conducted by analysing the $B_c^+ \to \pi^+\mu^+\mu^-$ process. The analysis uses proton-proton collision data collected with the LHCb detector between 2011 and 2018, corresponding to an integrated luminosity of $9\,\text{fb}^{-1}$. The signal signatures correspond to simultaneous peaks in the $\mu^+\mu^-$ and $\pi^+\mu^+\mu^-$ invariant masses. No evidence for an excess of events over background is observed for either signal decay mode. Upper limits are set on the branching fractions relative to that for $B_c^+ \to J/\psi\pi^+$ decays of

$$\mathcal{R}_{B^{*0}(\mu^+\mu^-)\pi^+/J/\psi\pi^+} < 3.8 \times 10^{-5}\,, \text{ and}$$
$$\mathcal{R}_{B_s^{*0}(\mu^+\mu^-)\pi^+/J/\psi\pi^+} < 5.0 \times 10^{-5}\,,$$

at 90% confidence level.

[†]Conference report prepared for the 12th edition of the Large Hadron Collider Physics Conference, Boston, USA, 3–7 June 2024. Contact authors: Fernando Abudinén, fernando.abudinen@cern.ch.

1 Introduction

Weak decays of the B^{*0} and B_s^{*0} excited vector mesons into leptonic final states offer the opportunity to search for possible deviations from Standard Model (SM) expectations. Unlike the weak leptonic decays of the B^0 and B_s^0 pseudoscalar mesons, the decays of excited vector mesons are not suppressed by the chiral structure of the SM weak interaction [1–3]. However, since the $B_{(s)}^{*0}$ mesons decay predominantly through the electromagnetic interaction, the branching fractions for their weak leptonic decays are highly suppressed in the SM. For example, the $B_s^{*0} \to \mu^+\mu^-$ branching fraction is expected in the SM to be around 10^{-11}, but could be enhanced due to physics beyond the SM [2].

Many experimental studies of the $B_{(s)}^0$ leptonic decays have been performed, with the latest results giving measurements of the $B_s^0 \to \mu^+\mu^-$ branching fraction and limits on the $B^0 \to \mu^+\mu^-$ rate that are consistent with SM expectations [4–7], as well as limits on the rates of $B_{(s)}^0 \to e^+e^-$ and $B_{(s)}^0 \to \tau^+\tau^-$ decays [8, 9]. However, there has not yet been any search for a $B_{(s)}^{*0} \to \ell^+\ell^-$ decay mode. In this report, the first search for the $B^{*0} \to \mu^+\mu^-$ and $B_s^{*0} \to \mu^+\mu^-$ decays is presented. The analysis is based on the data samples collected with the LHCb detector between 2011 and 2018, corresponding to an integrated luminosity of 9 fb^{-1} of proton-proton pp collisions at centre-of-mass energies of 7, 8 and 13 TeV. As discussed in Ref. [10], searches via prompt $B_{(s)}^{*0}$ production in LHC collisions are expected to be limited by the large amount of background from the pp interactions. The search is therefore performed instead via the $B_c^+ \to B_{(s)}^{*0}\pi^+$, $B_{(s)}^{*0} \to \mu^+\mu^-$ decay chain, subsequently denoted $B_c^+ \to B_{(s)}^{*0}(\mu^+\mu^-)\pi^+$. This is expected to be the most promising method as it exploits the displaced B_c^+-vertex signature to suppress background; a similar approach has recently been demonstrated in a search for the $D^{*0} \to \mu^+\mu^-$ decay [11]. The inclusion of charge conjugate processes is implied throughout the paper.

The analysis follows procedures from a recent search for nonresonant $B_c^+ \to \pi^+\mu^+\mu^-$ decays [12]. The results of that analysis include an upper limit on the ratio $\mathcal{B}(B_c^+ \to \pi^+\mu^+\mu^-)/\mathcal{B}(B_c^+ \to J/\psi\pi^+) < 1.9 \times 10^{-4}$ at 90% confidence level (CL) in the interval $15.0 < q^2 < 35.0\,\mathrm{GeV}^2/c^4$, where $q^2 = m^2(\mu^+\mu^-)$ is the square of the invariant mass of the dimuon system. That result can be used to set limits on the branching fraction products $\mathcal{B}(B_c^+ \to B_s^{*0}\pi^+) \times \mathcal{B}(B_s^{*0} \to \mu^+\mu^-)$ and $\mathcal{B}(B_c^+ \to B^{*0}\pi^+) \times \mathcal{B}(B^{*0} \to \mu^+\mu^-)$, since such decays would contribute in the relevant q^2 region. However, due to the narrow $B_{(s)}^{*0}$ width, significantly better experimental sensitivity can be obtained by a dedicated search with optimised selection requirements and fit strategy, as presented here. The previous result also implies that there is no significant contribution from nonresonant $B_c^+ \to \pi^+\mu^+\mu^-$ decays, and therefore this does not need to be considered as a source of background in the $B_{(s)}^{*0}$ search.

To search for $B_c^+ \to B_{(s)}^{*0}(\mu^+\mu^-)\pi^+$ signals, the reconstructed B_c^+-candidate invariant mass, $m(\mu^+\mu^-\pi^+)$, and the dimuon invariant mass, $m(\mu^+\mu^-)$, serve as discriminating observables in an extended unbinned maximum-likelihood fit. The analysis uses the $B_c^+ \to J/\psi(\mu^+\mu^-)\,\pi^+$ decay as normalisation mode. The signal yields, relative to that for the normalisation mode, are translated into branching fraction ratios through

$$\begin{aligned}\mathcal{R}_{B^{*0}_{(s)}(\mu^+\mu^-)\pi^+/J/\psi\pi^+} &\equiv \frac{\mathcal{B}(B_c^+\to B^{*0}_{(s)}(\mu^+\mu^-)\pi^+)}{\mathcal{B}(B_c^+\to J/\psi\pi^+)}\\ &= \frac{N_{B^{*0}_{(s)}\pi^+}}{N_{J/\psi\pi^+}}\cdot\frac{\varepsilon_{J/\psi\pi^+}}{\varepsilon_{B^{*0}_{(s)}\pi^+}}\cdot\mathcal{B}(J/\psi\to\mu^+\mu^-)\\ &= \alpha^{\mathrm{SES}}_{B^{*0}_{(s)}\pi^+}\cdot N_{B^{*0}_{(s)}\pi^+}\,,\end{aligned}\tag{1}$$

where N indicates the yield of the mode indicated in the subscript, ε indicates the efficiency determined from simulation with data-driven corrections, and $\mathcal{B}(J/\psi\to\mu^+\mu^-)$ is the known branching fraction of the $J/\psi\to\mu^+\mu^-$ decay [13]. The single-event-sensitivity $\alpha^{\mathrm{SES}}_{B^{*0}_{(s)}\pi^+}$ is the value of the ratio that would be obtained for one single signal decay.

2 Detector and simulation

The LHCb detector [14, 15] is a single-arm forward spectrometer covering the pseudorapidity range $2<\eta<5$, designed for the study of particles containing b or c quarks. The detector includes a high-precision tracking system consisting of a silicon-strip vertex detector surrounding the pp interaction region [16], a large-area silicon-strip detector located upstream of a dipole magnet with a bending power of about 4 T m, and three stations of silicon-strip detectors and straw drift tubes [17, 18] placed downstream of the magnet. The tracking system provides a measurement of the momentum, p, of charged particles with a relative uncertainty that varies from 0.5% at low momentum to 1.0% at 200 GeV/c. The minimum distance of a track to a primary pp collision vertex (PV), the impact parameter (IP), is measured with a resolution of $(15+29/p_{\mathrm{T}})\,\mu\mathrm{m}$, where p_{T} is the component of the momentum transverse to the beam, in GeV/c. Different types of charged hadrons are distinguished using information from two ring-imaging Cherenkov detectors [19]. Photons, electrons and hadrons are identified by a calorimeter system consisting of scintillating-pad and preshower detectors, an electromagnetic and a hadronic calorimeter. Muons are identified by a system composed of alternating layers of iron and multiwire proportional chambers [20].

The online event selection is performed by a trigger [21, 22], which consists of a hardware stage, based on information from the calorimeter and muon systems, followed by a two-level software stage, which reconstructs the full event. Candidate $B_c^+\to\pi^+\mu^+\mu^-$ decays are triggered as described in Ref. [11] for B^+ decays to the same final states. The hardware stage of the trigger selects events containing at least one muon with high p_{T}. The following software stage selects events containing at least one high-p_{T} muon detached from any PV. The events must contain at least one secondary vertex (formed by two or more of the final-state particles) that is also detached from any PV. Secondary vertices consistent with the decay of a b hadron are identified by multivariate algorithms [23, 24].

Simulation is used to optimise the event selection procedure, to model the shape of invariant-mass distributions and to estimate efficiencies accounting for the effects of the detector acceptance, reconstruction and selection criteria. In the simulation, pp collisions are generated using Pythia [25] with a specific LHCb configuration [26]. The production of B_c^+ mesons is simulated using the dedicated generator BcVegPy [27]. Decays of unstable particles are described by EvtGen [28], in which final-state radiation is generated using

Photos [29]. The interaction of the generated particles with the detector, and its response, are implemented using the Geant4 toolkit [30–32].

The B_c^+ candidates reconstructed in simulation are weighted to correct for discrepancies between data and simulation associated with the particle-identification [33], track-reconstruction [34] and hardware trigger [35] efficiencies. The simulation is also corrected such that the B_c^+ lifetime corresponds to the current experimental value [13, 36, 37]. Additional corrections are applied to account for discrepancies in B_c^+ production kinematics, event track multiplicity and other observables used in the selection of B_c^+ candidates. These corrections are obtained using a multivariate weighting algorithm [38], which is trained using $B_c^+ \to J/\psi\pi^+$ decays in background-subtracted data and simulation. After the corrections are applied, the simulated distributions of all variables used in the analysis are in good agreement with the data.

3 Candidate selection and background sources

The initial stages of the offline selection are identical to those for the recent search for nonresonant $B_c^+ \to \pi^+\mu^+\mu^-$ decays [12]. The B_c^+ candidates are formed from pairs of well-reconstructed oppositely charged tracks identified as muons together with a track identified as a pion. The tracks are required to form a good-quality vertex that is displaced from every PV. Each B_c^+ candidate must have a momentum vector that is aligned with the direction between one of the PVs and the B_c^+-candidate decay vertex.

Each B_c^+ candidate is required to have an invariant mass in the range $6150 < m(\pi^+\mu^+\mu^-) < 6700\,\mathrm{MeV}/c^2$. The expected signal resolution in $m(\pi^+\mu^+\mu^-)$ is about $20\,\mathrm{MeV}/c^2$. The dimuon invariant mass is calculated from the outcome of a kinematic fit in which the B_c^+-candidate invariant mass is constrained to the known B_c^+ mass [13] and the momentum vector is constrained to be consistent with the line of flight between the PV and the decay vertex, thereby improving the resolution. The dimuon invariant mass is required to be in the range $5225 < m(\mu^+\mu^-) < 5515\,\mathrm{MeV}/c^2$ for the signal modes and $3000 < m(\mu^+\mu^-) < 3200\,\mathrm{MeV}/c^2$ for the normalisation mode. The expected signal resolution in $m(\mu^+\mu^-)$ is about $4\,\mathrm{MeV}/c^2$.

Combinatorial background arising from random combinations of tracks is suppressed using a boosted decision tree (BDT) classifier [39, 40] that has been trained and validated to identify $B_c^+ \to \pi^+\mu^+\mu^-$ signal candidates irrespective of dimuon invariant mass [12]. The BDT classifier receives as inputs the p_{T} of the pion track, the p_{T} of the muon track with highest p_{T}, the IPs of the muon tracks and the B_c^+ candidate, the B_c^+ flight distance, the vertex quality of the B_c^+ candidate, and the largest distance of closest approach between any two of the final-state particles.

Further suppression of combinatorial background is obtained by applying a requirement on the cosine of the helicity angle θ_l, which is defined as the angle between the μ^+ direction and the direction opposite of the B_c^+ momentum in the dimuon rest frame. This has additional discrimination power since the signal follows a $1 - \cos^2\theta_l$ distribution while the combinatorial background sharply peaks at $\cos\theta_l \approx \pm 1$.

Requirements on the BDT classifier output, the absolute value of $\cos\theta_l$, and variables characterising the charged pion particle identification are optimised simultaneously. The optimisation is based on a grid search to obtain the best signal sensitivity using the figure of merit $\varepsilon/(5/2 + \sqrt{N_{\mathrm{B}}})$ [41], where ε is the signal efficiency and N_{B} is the expected number of background candidates in the signal region. The figure of merit is evaluated separately for $B_c^+ \to B^{*0}(\mu^+\mu^-)\pi^+$ and $B_c^+ \to B_s^{*0}(\mu^+\mu^-)\pi^+$ decays. The signal region for each decay mode corresponds to a two-dimensional range in $m(\pi^+\mu^+\mu^-)$ and $m(\mu^+\mu^-)$ of about ±3 times the expected resolution in each dimension, centred at the expected two-dimensional peak position [13]. The expected background yield is estimated by fitting a background-only model to the dataset excluding the region $6215 < m(\pi^+\mu^+\mu^-) < 6335\,\mathrm{MeV}/c^2$.

The figures of merit for both $B_c^+ \to B^{*0}(\mu^+\mu^-)\pi^+$ and $B_c^+ \to B_s^{*0}(\mu^+\mu^-)\pi^+$ decays have maximum values at the same grid point. With the optimised requirements, the classifier has a combinatorial background rejection power of 99%, whilst retaining 65% of signal decays. The optimised angular selection, corresponding to $|\cos\theta_l| < 0.90$, further rejects about 30% of the background whilst keeping about 98% of signal decays. The particle-identification requirements have a pion efficiency around 90%, with a kaon misidentification rate around 10%. The particle-identification requirements applied to the muon candidates have an efficiency around 99%, with a pion misidentification rate below 1%. The same selection requirements are used for signal and normalisation modes to reduce potential systematic biases on the measurement of branching fraction ratios. After applying the selection requirements each selected event contains only one B_c^+ candidate.

Backgrounds from partially reconstructed decays such as $B_c^+ \to J/\psi\rho^+(\pi^+\pi^0)$ [42] for the normalisation mode have a reconstructed B_c^+-candidate invariant mass that lies more than $100\,\mathrm{MeV}/c^2$ below the known B_c^+ mass [13]. These sources of background predominantly populate a region outside, but have a tail that extends into, the fit range used in the analysis. This is also true for backgrounds such as $B_c^+ \to \rho^+\mu^+\mu^-$ for the signal modes, which were found to be negligible in the search for nonresonant $B_c^+ \to \pi^+\mu^+\mu^-$ decays [12]. This contribution is therefore neglected in the fit for the signal modes, but is accounted for in the normalisation mode fit. Processes with a missing neutrino or two or more missing massive particles can also be a source of partially reconstructed background, but their contributions are negligible in the fit range.

Contributions from hadronic backgrounds such as $B_c^+ \to \pi^+\pi^-\pi^+$ decays, where two pions are mistakenly identified as muons, were found to be negligible in the search for nonresonant $B_c^+ \to \pi^+\mu^+\mu^-$ decays [12] and are therefore neglected. Similarly, possible contributions from the resonant $B_c^+ \to J/\psi\pi^+$ or $B_c^+ \to \psi(2S)\pi^+$ decays, where the pion is mistakenly identified as a muon and vice versa, were studied using simulation and data and found to be negligible after applying the selection requirements.

For the normalisation mode, misidentified background can arise from the $B_c^+ \to J/\psi K^+$ mode. The branching fraction for this decay is Cabibbo-suppressed with respect to that for the $B_c^+ \to J/\psi\pi^+$ decay, and their ratio has been measured to be $0.079 \pm 0.007 \pm 0.003$ [43]. This background is further suppressed by the particle-identification requirements, but nonetheless is accounted for in the normalisation mode fit.

4 Invariant-mass fits

The normalisation $B_c^+ \to J/\psi(\mu^+\mu^-)\,\pi^+$ yield is determined from a one-dimensional extended unbinned maximum-likelihood fit to the $m(\pi^+\mu^+\mu^-)$ distribution of candidates in the range $3000 < m(\mu^+\mu^-) < 3200\,\mathrm{MeV}/c^2$. The normalisation mode also provides correction factors that account for discrepancies between data and simulation in the signal peak positions and widths. The relevant factors for the dimuon signal shape are obtained from an additional maximum-likelihood fit to the $m(\mu^+\mu^-)$ distribution. The B_c^+-candidate invariant-mass and dimuon invariant-mass fits to the normalisation mode are independent of each other. A two-dimensional fit is avoided since possible correlations in the tail regions of the two observables could result in a non-negligible fit bias given the large sample size.

For the B_c^+-candidate invariant-mass fits, the fit model includes four components: signal $B_c^+ \to J/\psi\pi^+$ decays, misidentified $B_c^+ \to J/\psi K^+$ decays, partially reconstructed background from $B_c^+ \to J/\psi\rho^+$ decays and combinatorial background. The signal, misidentified and partially reconstructed backgrounds are each modelled by the sum of two Gaussian functions, one of which has power-law tails [44]. The tail parameters of each distribution are fixed from simulation. The peak position and width of the distributions are allowed to vary in the fit to the data by a global offset and scale factor that is shared between these three components. The combinatorial background model is an exponential function with an exponent that is allowed to vary. In total, the fit includes seven parameters: the yields of the four components, the global peak position shift and width scaling factor, and the exponent of the combinatorial background. The yield for misidentified $B_c^+ \to J/\psi K^+$ decays is allowed to vary with respect to the yield for the $B_c^+ \to J/\psi\pi^+$ decays within a Gaussian constraint based on the expected misidentification rate [33] and the measured branching fraction ratio [43].

For the dimuon invariant-mass fit, the fit model includes a signal and a combinatorial background component. The signal is modelled by a Gaussian function with power-law tails, while the background is modelled by a first-order polynomial function. The tail parameters of the signal model are fixed from $B_c^+ \to J/\psi\pi^+$ simulation. The signal peak position and width are allowed to vary in the fit to the data through an offset and a scale factor. The dimuon-mass fit model includes five fit parameters: the yields for the two components, the shift of peak position and width scaling factor and the slope of the combinatorial background.

Figure 1 shows the dimuon and B_c^+-candidate invariant-mass distributions of selected $B_c^+ \to J/\psi\pi^+$ candidates. The B_c^+-candidate invariant-mass fit converges to a yield of 6213 ± 89 decays, where the uncertainty is statistical only.

The dimuon invariant-mass distribution in data can receive contributions from J/ψ de-

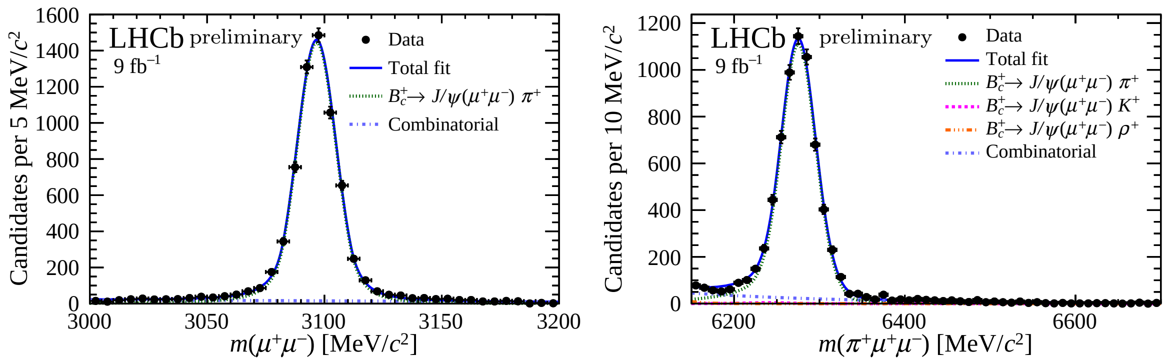

Figure 1: Reconstructed (left) $\mu^+\mu^-$ and (right) $\pi^+\mu^+\mu^-$ invariant-mass distributions for the selected $B_c^+ \to J/\psi(\mu^+\mu^-)\pi^+$ candidates, with results of the fit superimposed.

cays that do not stem from the $B_c^+ \to J/\psi\pi^+$ process. This background contribution could affect the fit results for the shift and width scaling factors. To check this and also the effect of dependencies in the tails between B_c^+-mass and dimuon mass distributions, the fit is repeated restricting the B_c^+-candidates to the region $6215 < m(\pi^+\mu^+\mu^-) < 6335\,\mathrm{MeV}/c^2$. The results for the shift and width scaling factor obtained from this fit agree within uncertainties with the results obtained from the nominal fit.

The signal $B_c^+ \to B^{*0}(\mu^+\mu^-)\pi^+$ and $B_c^+ \to B_s^{*0}(\mu^+\mu^-)\pi^+$ yields are determined from a two-dimensional extended unbinned maximum-likelihood fit to the $m(\mu^+\mu^-)$ and $m(\pi^-\mu^+\mu^-)$ distributions. The fit model includes three components: signal $B_c^+ \to B^{*0}(\mu^+\mu^-)\pi^+$ decays, signal $B_c^+ \to B_s^{*0}(\mu^+\mu^-)\pi^+$ decays and combinatorial background. For each component, the total model is the product of the respective dimuon and B_c^+-candidate invariant-mass models. The models for the signal components are validated using simulation. The two fit observables are found to have no significant correlation between them in simulation or sideband data and are therefore treated as uncorrelated.

For the signal components, the dimuon and the B_c^+-candidate invariant-mass distributions are each modelled using a Gaussian function with power-law tails on both sides of the peak. The tail parameters are fixed to the values obtained from simulation. The signal dimuon and B_c^+-candidate invariant-mass models each include a global shift of peak position and a global scaling factor for the width of the distribution, relative to the values found in simulation.

For the combinatorial background, the dimuon and the B_c^+-candidate invariant-mass distributions are modelled using a linear function and an exponential function, respectively. The respective dimuon and the B_c^+-candidate invariant-mass slopes are allowed to vary in the fit to data.

In total, the fit includes five free parameters: the yields for each component and the two parameters of the combinatorial background model. The global peak position shift and width scaling factor for each of the dimuon and B_c^+-candidate invariant-mass models are constrained to be consistent with values obtained from fits to the $B_c^+ \to J/\psi(\mu^+\mu^-)\,\pi^+$ candidates.

Figure 2 shows the dimuon and B_c^+-candidate invariant-mass distributions of selected $B_c^+ \to B_{(s)}^{*0}(\mu^+\mu^-)\pi^+$ candidates, with results of the fit superimposed. Figure 3 shows the two-dimensional distribution of selected candidates. The yields for the $B_c^+ \to B^{*0}(\mu^+\mu^-)\pi^+$ and $B_c^+ \to B_s^{*0}(\mu^+\mu^-)\pi^+$ decays are consistent with zero. Table 1 summarises the yields obtained from the fit. The correlation between the two signal yields is 1.2%.

Table 1: Yields obtained from the fit to data described in the text, with statistical uncertainties only.

Component	Yield
$B_c^+ \to B^{*0}(\mu^+\mu^-)\pi^+$	$-0.4\,^{+1.9}_{-1.1}$
$B_c^+ \to B_s^{*0}(\mu^+\mu^-)\pi^+$	$0.4\,^{+2.2}_{-1.3}$
Combinatorial bkg.	282 ± 17

Table 2: Input parameters used in the estimation of the ratio $\mathcal{R}_{B^{*0}_{(s)}(\mu^+\mu^-)\pi^+/J/\psi\pi^+}$, with statistical and systematic uncertainties added in quadrature.

Parameter	Value
$\mathcal{B}\,(J/\psi \to \mu^+\mu^-)$	$(59.61 \pm 0.33) \times 10^{-3}$ [13]
$\varepsilon_{J/\psi\pi^+}/\varepsilon_{B^{*0}\pi^+}$	1.09 ± 0.05
$\varepsilon_{J/\psi\pi^+}/\varepsilon_{B^{*0}_s\pi^+}$	1.18 ± 0.05
$N_{J/\psi\pi^+}$	6213 ± 93

5 Efficiencies and systematic uncertainties

Table 2 summarises the parameters entering the determination of the single event sensitivities in Eq. (1), with statistical and systematic uncertainties added in quadrature.

The efficiency ratios between signal and normalisation modes are obtained from simulation accounting for the geometrical acceptance of the detector as well as effects related to the triggering, reconstruction and selection of the B_c^+ candidates. The uncertainties on the efficiency ratios take into account the simulation sample size, uncertainties on the weights applied to the simulation, the matching between reconstructed and generated particles in the simulation, variations of the software trigger requirements, and the uncertainty on the known B_c^+ lifetime. All variations are made consistently for the signal and normalisation modes to avoid overestimation of the uncertainty on the efficiency ratio.

The systematic uncertainties associated with the weights are evaluated by varying all weights within their uncertainties and by varying the binning scheme used to estimate them. The systematic uncertainty associated with the multivariate weighting algorithm (see Sec. 2) is evaluated by comparing the results obtained with the default and with an alternative algorithm. The default algorithm is trained to correct for discrepancies between data and simulation associated with the event track multiplicity and with the transverse momentum and the vertex quality of the B_c^+ candidates. The alternative algorithm is trained using the impact parameter significance of the two muons as additional inputs.

The systematic uncertainty associated with the matching between reconstructed and generated particles in the simulation is evaluated by comparing the efficiencies obtained

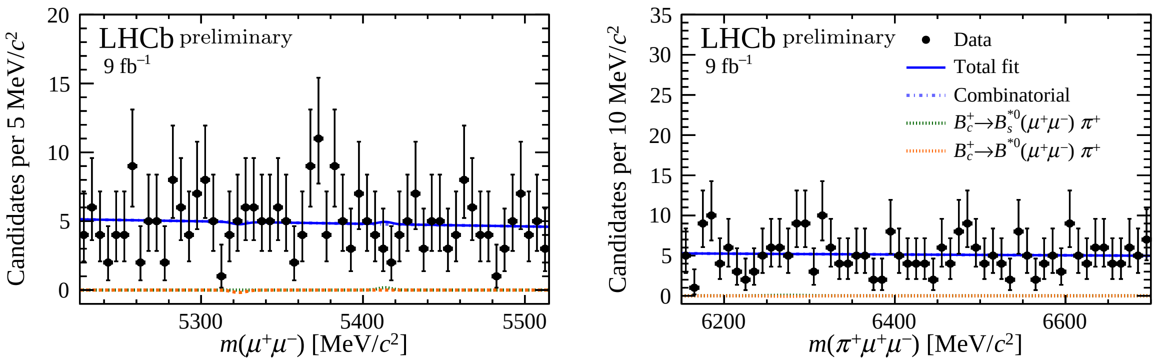

Figure 2: Reconstructed (left) $\mu^+\mu^-$ and (right) $\pi^+\mu^+\mu^-$ invariant-mass distributions for the selected $B_c^+ \to B^{*0}_{(s)}(\mu^+\mu^-)\pi^+$ candidates, with results of the fit superimposed.

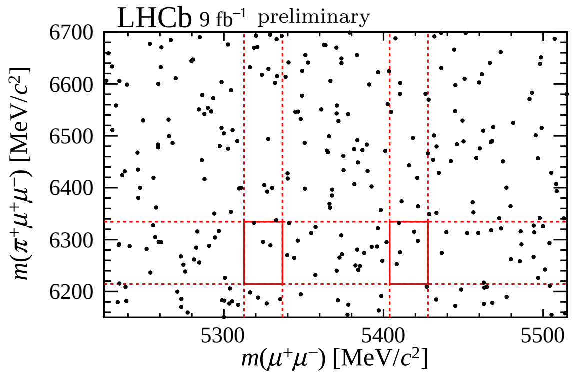

Figure 3: Two-dimensional distribution of $\mu^+\mu^-$ invariant mass versus $\pi^+\mu^+\mu^-$ invariant mass for the selected $B_c^+ \to B_{(s)}^{*0}(\mu^+\mu^-)\pi^+$ candidates. The areas delimited by the full red lines correspond to ranges of about ±3 times the experimental resolution around the expected signal-peak positions in each dimension.

including or excluding B candidates for which one or more decay products are not correctly matched. The systematic uncertainty associated with variations of the software trigger requirements that are not reproduced by the simulation is evaluated by comparing the efficiencies obtained by applying the tightest thresholds and by applying average thresholds within each data-taking period. The systematic uncertainty associated with the B_c^+ lifetime is evaluated by varying the B_c^+ lifetime in simulation within its uncertainties [13].

A further systematic effect associated with the track reconstruction [34] can arise due to the possible difference in hadronic interactions for the pion tracks in the signal and the normalisation modes (due to the kinematic differences between the decays) and discrepancies between data and simulation in the detector material. This effect is studied in simulation and data and is found to have a negligible impact.

The effect of the multivariate weighting algorithm has the largest impact on the systematic uncertainty of the efficiency ratio. The remaining systematic uncertainties cancel out almost completely in the determination of the efficiency ratios and are smaller than the statistical uncertainties.

The normalisation mode yield obtained in the previous section can be affected by the fit model choice and by the assumption of the polarisation of the partially reconstructed backgrounds. To study the effect of the fit model choice, each fit is performed in three configurations: using the baseline fit model and using two alternative fit models. In the two alternative fit models, the analytical function used for the combinatorial background is replaced by a sigmoid function. In the first alternative model the same parametrisation as in the nominal model is kept for the other fit components, while in the second alternative model the $B_c^+ \to J/\psi\pi^+$ and the misidentified background models are replaced by a Hypathia function [45] and the model for the partially reconstructed background is replaced by a Gaussian function with a power-law tail to the right side of the distribution. For the normalisation mode yield, the largest difference between the results obtained with the baseline and alternative models is assigned as systematic uncertainty. For the global peak shift and width correction factors, the model choice is found to have a negligible impact.

In the nominal normalisation mode fit, the ρ^+ meson in the $B_c^+ \to J/\psi\rho^+$ partially reconstructed background is assumed to be unpolarised. However, the polarisation of the

ρ^+ meson can affect the momentum of the missing pion and hence the B_c^+-candidate mass shape of the partially reconstructed backgrounds. The fit is therefore repeated assuming either full longitudinal or full transverse ρ^+ polarisation. The difference in the results for the two configurations is found to be negligible.

6 Results for relative branching fractions

The signal yields in the fit model described in Sec. 4 are parametrised in terms of branching fraction ratios $\mathcal{R}_{B^{*0}_{(s)}(\mu^+\mu^-)\pi^+/J/\psi\pi^+}$ using Eq. (1). The systematic uncertainties associated with the single-event sensitivities are accounted for through Gaussian constraints in the fit. Using the parameters in Table 2 to calculate the single-event-sensitivities gives $\alpha^{\rm SES}_{B^{*0}\pi^+} = (1.04 \pm 0.05) \times 10^{-5}$ and $\alpha^{\rm SES}_{B^{*0}_s\pi^+} = (1.13 \pm 0.05) \times 10^{-5}$ taking statistical and systematic uncertainties into account. Including all constraints, the fit yields

$$\begin{aligned}\mathcal{R}_{B^{*0}(\mu^+\mu^-)\pi^+/J/\psi\pi^+} &= (-0.44^{+1.99}_{-1.12}) \times 10^{-5}\,,\\ \mathcal{R}_{B^{*0}_s(\mu^+\mu^-)\pi^+/J/\psi\pi^+} &= \quad (0.43^{+2.45}_{-1.41}) \times 10^{-5}\,.\end{aligned}$$

To assess the impact of the systematic uncertainties, the fits are repeated fixing the nuisance parameters to their central values. The difference in the uncertainties between the two configurations is around 10^{-7}, showing that the impact of the systematic uncertainties is negligible.

Upper limits on the branching fraction ratios are obtained following the Feldman–Cousins prescription [46]: pseudoexperiments are generated for various values of $\mathcal{R}_{B^{*0}_{(s)}(\mu^+\mu^-)\pi^+/J/\psi\pi^+}$ and the distributions of the measured $\mathcal{R}_{B^{*0}_{(s)}(\mu^+\mu^-)\pi^+/J/\psi\pi^+}$ values in the pseudoexperiments are used to form confidence belts. Nuisance parameters are varied within their uncertainties in the generation of the pseudoexperiments. The scan to obtain limits for $\mathcal{R}_{B^{*0}(\mu^+\mu^-)\pi^+/J/\psi\pi^+}$ is performed assuming that $\mathcal{R}_{B^{*0}_s(\mu^+\mu^-)\pi^+/J/\psi\pi^+}$ is zero and vice versa. This assumption does not impact the obtained limits as the correlation between the signal yields is negligible. Figure 4 shows confidence belts at 90% and 95% confidence level (CL). Using the results obtained from the fit to data yields

$$\begin{aligned}\mathcal{R}_{B^{*0}(\mu^+\mu^-)\pi^+/J/\psi\pi^+} &< 3.8\,(5.2) \times 10^{-5} \text{ at } 90\ (95)\%\,\text{CL}\,,\\ \mathcal{R}_{B^{*0}_s(\mu^+\mu^-)\pi^+/J/\psi\pi^+} &< 5.0\,(6.3) \times 10^{-5} \text{ at } 90\ (95)\%\,\text{CL}\,.\end{aligned}$$

As further checks the procedure is repeated restricting the signal yield to positive values, or replacing in the fit model the signal parametrisation with the sum of two Gaussian functions, one with power-law tails. No significant changes in the obtained upper limits are found.

As a further cross-check, the ratio $\mathcal{B}(B_c^+ \to \psi(2S)(\mu^+\mu^-)\pi^+)/\mathcal{B}(B_c^+ \to J/\psi(\mu^+\mu^-)\pi^+)$ is measured following the same analysis procedure as in Ref. [12], but applying the BDT classifier, $\cos\theta_l$ and particle-identification requirements optimised for this work. The measured value corresponding to 0.279 ± 0.025, where the uncertainty is only statistical, agrees with previously published measurements of this quantity [12, 47, 48].

7 Summary

A search is performed for the very rare $B^{*0} \to \mu^+\mu^-$ and $B_s^{*0} \to \mu^+\mu^-$ decays by analysing $B_c^+ \to \pi^+\mu^+\mu^-$ decays. The analysis uses proton-proton collision data collected with the

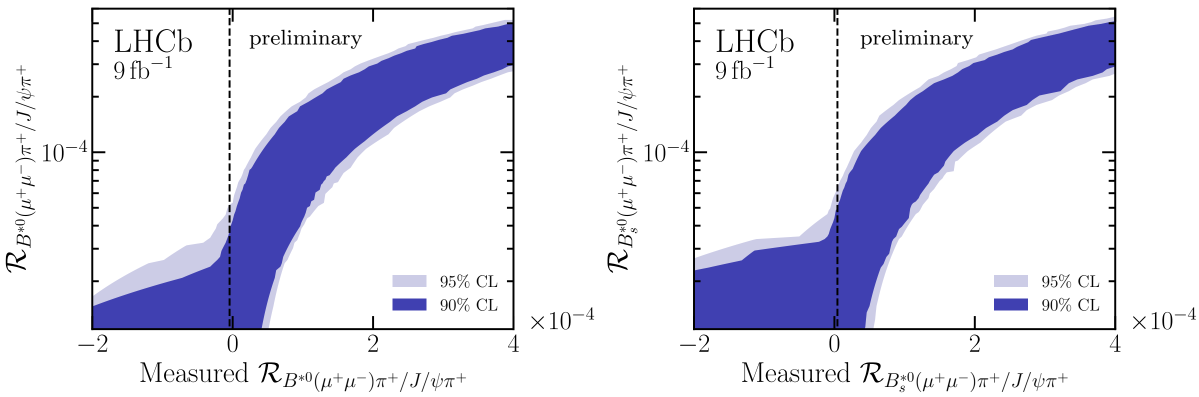

Figure 4: Confidence belts generated using pseudoexperiments according to the Feldman–Cousins prescription [46]. The vertical black line shows the results of the fit to data.

LHCb detector between 2011 and 2018, corresponding to an integrated luminosity of 9 fb^{-1}. No evidence for an excess of signal events over background is observed for the two decay modes and an upper limit is set on the branching fraction ratios

$$\mathcal{R}_{B^{*0}(\mu^+\mu^-)\pi^+/J/\psi\pi^+} < 3.8\times 10^{-5}\,,$$
$$\mathcal{R}_{B_s^{*0}(\mu^+\mu^-)\pi^+/J/\psi\pi^+} < 5.0\times 10^{-5}\,,$$

at 90% confidence level. These are the first limits on the ratios of these decays. Once measurements of the ratio $\mathcal{B}(B_c^+\to B_{(s)}^{*0}\pi^+)/\mathcal{B}(B_c^+\to J/\psi\pi^+)$ become available, it will be possible to translate these results into limits on the $B_{(s)}^{*0}\to\mu^+\mu^-$ branching fractions.

References

[1] G. Buchalla, A. J. Buras, and M. E. Lautenbacher, *Weak decays beyond leading logarithms*, Rev. Mod. Phys. **68** (1996) 1125, arXiv:hep-ph/9512380.

[2] B. Grinstein and J. Martin Camalich, *Weak decays of excited B mesons*, Phys. Rev. Lett. **116** (2016) 141801, arXiv:1509.05049.

[3] A. Khodjamirian, T. Mannel, and A. A. Petrov, *Direct probes of flavor-changing neutral currents in e^+e^- collisions*, JHEP **11** (2015) 142, arXiv:1509.07123.

[4] LHCb collaboration, R. Aaij *et al.*, *Analysis of neutral B-meson decays into two muons*, Phys. Rev. Lett. **128** (2022) 041801, arXiv:2108.09284.

[5] LHCb collaboration, R. Aaij *et al.*, *Measurement of the $B_s^0\to\mu^+\mu^-$ decay properties and search for the $B^0\to\mu^+\mu^-$ and $B_s^0\to\mu^+\mu^-\gamma$ decays*, Phys. Rev. **D105** (2022) 012010, arXiv:2108.09283.

[6] CMS collaboration, A. Tumasyan *et al.*, *Measurement of the $B_s^0\to\mu^+\mu^-$ decay properties and search for the $B^0\to\mu^+\mu^-$ decay in proton-proton collisions at $\sqrt{s}=13$ TeV*, Phys. Lett. **B842** (2023) 137955, arXiv:2212.10311.

[7] ATLAS collaboration, M. Aaboud *et al.*, *Study of the rare decays of B_s^0 and B^0 mesons into muon pairs using data collected during 2015 and 2016 with the ATLAS detector*, JHEP **04** (2019) 098, arXiv:1812.03017.

[8] LHCb collaboration, R. Aaij *et al.*, *Search for the rare decays $B_s^0 \to e^+e^-$ and $B^0 \to e^+e^-$*, Phys. Rev. Lett. **124** (2020) 211802, arXiv:2003.03999.

[9] LHCb collaboration, R. Aaij *et al.*, *Search for the decays $B_s^0 \to \tau^+\tau^-$ and $B^0 \to \tau^+\tau^-$*, Phys. Rev. Lett. **118** (2017) 251802, arXiv:1703.02508.

[10] F. Abudinén, T. Blake, U. Egede, and T. Gershon, *Prospects for studies of $D^{*0} \to \mu^+\mu^-$ and $B_{(s)}^{*0} \to \mu^+\mu^-$ decays*, Eur. Phys. J. **C82** (2022) 459, arXiv:2202.03916.

[11] LHCb collaboration, R. Aaij *et al.*, *Search for $D^{*0} \to \mu^+\mu^-$ in $B^- \to \pi^-\mu^+\mu^-$ decays*, Eur. Phys. J. **C83** (2023) 666, arXiv:2304.01981.

[12] LHCb collaboration, R. Aaij *et al.*, *Search for $B_c^+ \to \pi^+\mu^+\mu^-$ decays and measurement of the branching fraction ratio $\mathcal{B}(B_c^+ \to \psi(2S)\pi^+)/\mathcal{B}(B_c^+ \to J/\psi\pi^+)$*, Eur. Phys. J. **C84** (2024) 468, arXiv:2312.12228.

[13] Particle Data Group, R. L. Workman *et al.*, *Review of particle physics*, Prog. Theor. Exp. Phys. **2022** (2022) 083C01.

[14] LHCb collaboration, A. A. Alves Jr. *et al.*, *The LHCb detector at the LHC*, JINST **3** (2008) S08005.

[15] LHCb collaboration, R. Aaij *et al.*, *LHCb detector performance*, Int. J. Mod. Phys. **A30** (2015) 1530022, arXiv:1412.6352.

[16] R. Aaij *et al.*, *Performance of the LHCb Vertex Locator*, JINST **9** (2014) P09007, arXiv:1405.7808.

[17] R. Arink *et al.*, *Performance of the LHCb Outer Tracker*, JINST **9** (2014) P01002, arXiv:1311.3893.

[18] P. d'Argent *et al.*, *Improved performance of the LHCb Outer Tracker in LHC Run 2*, JINST **12** (2017) P11016, arXiv:1708.00819.

[19] M. Adinolfi *et al.*, *Performance of the LHCb RICH detector at the LHC*, Eur. Phys. J. **C73** (2013) 2431, arXiv:1211.6759.

[20] A. A. Alves Jr. *et al.*, *Performance of the LHCb muon system*, JINST **8** (2013) P02022, arXiv:1211.1346.

[21] R. Aaij *et al.*, *The LHCb trigger and its performance in 2011*, JINST **8** (2013) P04022, arXiv:1211.3055.

[22] R. Aaij *et al.*, *Design and performance of the LHCb trigger and full real-time reconstruction in Run 2 of the LHC*, JINST **14** (2019) P04013, arXiv:1812.10790.

[23] V. V. Gligorov and M. Williams, *Efficient, reliable and fast high-level triggering using a bonsai boosted decision tree*, JINST **8** (2013) P02013, arXiv:1210.6861.

[24] T. Likhomanenko *et al.*, *LHCb topological trigger reoptimization*, J. Phys. Conf. Ser. **664** (2015) 082025, arXiv:1510.00572.

[25] T. Sjöstrand, S. Mrenna, and P. Skands, *A brief introduction to PYTHIA 8.1*, Comput. Phys. Commun. **178** (2008) 852, arXiv:0710.3820.

[26] I. Belyaev *et al.*, *Handling of the generation of primary events in Gauss, the LHCb simulation framework*, J. Phys. Conf. Ser. **331** (2011) 032047.

[27] C.-H. Chang, J.-X. Wang, and X.-G. Wu, *BCVEGPY2.0: An upgraded version of the generator BCVEGPY with the addition of hadroproduction of the P-wave B_c^+ states*, Comput. Phys. Commun. **174** (2006) 241, arXiv:hep-ph/0504017.

[28] D. J. Lange, *The EvtGen particle decay simulation package*, Nucl. Instrum. Meth. **A462** (2001) 152.

[29] N. Davidson, T. Przedzinski, and Z. Was, *PHOTOS interface in C++: Technical and physics documentation*, Comp. Phys. Comm. **199** (2016) 86, arXiv:1011.0937.

[30] Geant4 collaboration, J. Allison *et al.*, *Geant4 developments and applications*, IEEE Trans. Nucl. Sci. **53** (2006) 270; Geant4 collaboration, S. Agostinelli *et al.*, *Geant4: A simulation toolkit*, Nucl. Instrum. Meth. **A506** (2003) 250.

[31] M. Clemencic *et al.*, *The LHCb simulation application, Gauss: Design, evolution and experience*, J. Phys. Conf. Ser. **331** (2011) 032023.

[32] D. Müller, M. Clemencic, G. Corti, and M. Gersabeck, *ReDecay: A novel approach to speed up the simulation at LHCb*, Eur. Phys. J. **C78** (2018) 1009, arXiv:1810.10362.

[33] R. Aaij *et al.*, *Selection and processing of calibration samples to measure the particle identification performance of the LHCb experiment in Run 2*, Eur. Phys. J. Tech. Instr. **6** (2019) 1, arXiv:1803.00824.

[34] LHCb collaboration, R. Aaij *et al.*, *Measurement of the track reconstruction efficiency at LHCb*, JINST **10** (2015) P02007, arXiv:1408.1251.

[35] S. Tolk, J. Albrecht, F. Dettori, and A. Pellegrino, *Data driven trigger efficiency determination at LHCb*, LHCb-PUB-2014-039, 2014.

[36] LHCb collaboration, R. Aaij *et al.*, *Measurement of the B_c^+ meson lifetime using $B_c^+ \to J/\psi\mu^+\nu_\mu X$ decays*, Eur. Phys. J. **C74** (2014) 2839, arXiv:1401.6932.

[37] LHCb collaboration, R. Aaij *et al.*, *Measurement of the lifetime of the B_c^+ meson using the $B_c^+ \to J/\psi\pi^+$ decay mode*, Phys. Lett. **B742** (2015) 29, arXiv:1411.6899.

[38] A. Rogozhnikov, *Reweighting with boosted decision trees*, J. Phys. Conf. Ser. **762** (2016) 012036, arXiv:1608.05806, https://github.com/arogozhnikov/hep_ml.

[39] L. Breiman, J. H. Friedman, R. A. Olshen, and C. J. Stone, *Classification and regression trees*, Wadsworth international group, Belmont, California, USA, 1984.

[40] T. Chen and C. Guestrin, *XGBoost: A scalable tree boosting system*, in *Proceedings of the 22nd ACM SIGKDD International Conference on Knowledge Discovery and Data Mining*, KDD '16, (New York, NY, USA), 785–794, ACM, 2016.

[41] G. Punzi, *Sensitivity of searches for new signals and its optimization*, eConf **C030908** (2003) MODT002, arXiv:physics/0308063.

[42] LHCb collaboration, R. Aaij *et al.*, *Observation of the $B_c^+ \to J/\psi\pi^+\pi^0$ decay*, JHEP **02** (2024) 151, arXiv:2402.05523.

[43] LHCb collaboration, R. Aaij *et al.*, *Measurement of the ratio of branching fractions $\mathcal{B}(B_c^+ \to J/\psi K^+)/\mathcal{B}(B_c^+ \to J/\psi\pi^+)$*, JHEP **09** (2016) 153, arXiv:1607.06823.

[44] T. Skwarnicki, *A study of the radiative cascade transitions between the Upsilon-prime and Upsilon resonances*, PhD thesis, Institute of Nuclear Physics, Krakow, 1986, DESY-F31-86-02.

[45] D. Martínez Santos and F. Dupertuis, *Mass distributions marginalized over per-event errors*, Nucl. Instrum. Meth. **A764** (2014) 150, arXiv:1312.5000.

[46] G. J. Feldman and R. D. Cousins, *A unified approach to the classical statistical analysis of small signals*, Phys. Rev. **D57** (1998) 3873, arXiv:physics/9711021.

[47] LHCb collaboration, R. Aaij *et al.*, *Observation of the decay $B_c^+ \to \psi(2S)\pi^+$*, Phys. Rev. **D87** (2013) 071103(R), arXiv:1303.1737.

[48] LHCb collaboration, R. Aaij *et al.*, *Measurement of the branching fraction ratio $\mathcal{B}(B_c^+ \to \psi(2S)\pi^+)/\mathcal{B}(B_c^+ \to J/\psi\pi^+)$*, Phys. Rev. **D92** (2015) 057007, arXiv:1507.03516.